Building and Environment 177 (2020) 106866

Contents lists available at ScienceDirect

Building and Environment

journal homepage: http://www.elsevier.com/locate/buildenv

Hygrothermal characterization and modeling of cross-laminated timber in the building envelope

Steven Kordziel [a], Samuel V. Glass [b,*], Charles R. Boardman [b], Robert A. Munson [b], Samuel L. Zelinka [b], Shiling Pei [a], Paulo Cesar Tabares-Velasco [c]

[a] Department of Civil and Environmental Engineering, Colorado School of Mines, 1500 Illinois St., Golden, CO, 80401, USA
[b] Building and Fire Sciences, Forest Products Laboratory, USDA Forest Service, 1 Gifford Pinchot Dr., Madison, WI, 53726, USA
[c] Department of Mechanical Engineering, Colorado School of Mines, 1500 Illinois St., Golden, CO, 80401, USA

ARTICLE INFO

Keywords:
Cross-laminated timber
Building envelope
Hygrothermal modeling
Moisture performance
Water uptake
Hygric redistribution

ABSTRACT

Cross-laminated timber (CLT) is a type of mass timber panel used in floor, wall, and roof assemblies. An important consideration in design and construction of timber buildings is moisture durability. This study characterized the hygrothermal performance of CLT panels with laboratory measurements at multiple scales, field measurements, and modeling. The CLT panels consisted of five layers, four with spruce-pine-fir lumber and one with Douglas-fir lumber. Laboratory characterization involved measurements on small specimens that included material from only one or two layers and large specimens that included all five layers of the CLT panel. Water absorption was measured with panel specimens partially immersed in water, and a new method was developed where panels were exposed to ponded water on the top surface. This configuration gave a higher rate of water uptake than the partial immersion test. The rate of drying was much slower when the wetted surface was covered with an impermeable membrane. Measured hygrothermal properties were implemented in a one-dimensional transient hygrothermal model. Simulation of water uptake indicated that vapor diffusion had a significant contribution in parallel with liquid transport. A simple approximation for liquid transport coefficients, with identical coefficients for suction and redistribution, was adequate for simulating panel-scale wetting and drying. Finally, hygrothermal simulation of a CLT roof assembly that had been monitored in a companion field study showed agreement in most cases within the sensor uncertainty. Although the hygrothermal properties are particular to the wood species and CLT panels investigated here, the modeling approach is broadly applicable.

1. Introduction

Cross-laminated timber (CLT) is a wood composite panel consisting of multiple layers of lumber that are laid and adhered orthogonally [1,2]. CLT panels can be used in many structural applications, the most common being floor, wall, and roof assemblies. Innovative mass timber buildings featuring CLT, with heights between eight and 18 stories, have been constructed recently in various locations worldwide [3]. The low carbon footprint, construction efficiency, and economic competitiveness of mass timber systems have made them viable alternatives and, in some cases, superior to conventional steel and concrete structural systems [1–4]. CLT panels in exterior walls and roofs are part of the building envelope, separating the interior and exterior environments. Moisture management is essential in buildings with timber structural members because elevated moisture levels reduce the structural properties and can lead to dimensional instability, physical deterioration (e.g., cracking and delamination), biological deterioration (e.g., fungal growth, bacteria, and insects), and chemical deterioration (e.g., corrosion of metal connections). Characterizing the response of CLT to environmental conditions is necessary for informed design and construction practices that yield safe and durable mass timber buildings.

General guidance on use of CLT in the building envelope has been published in several handbooks in North America [2,5–7]. These handbooks caution that when CLT panels are exposed to weather, the panels may absorb a large amount of moisture and subsequent drying may be slow. At the time of manufacturing, the moisture content (MC, mass of moisture expressed as a percentage of dry material mass) in CLT panels is controlled to between 9% and 15% [8]. Panels are usually wrapped during transport and storage; one study found that CLT moisture content did not change significantly from the manufacturing plant

* Corresponding author.
E-mail address: samuel.v.glass@usda.gov (S.V. Glass).

https://doi.org/10.1016/j.buildenv.2020.106866
Received 24 January 2020; Received in revised form 16 March 2020; Accepted 21 March 2020
Available online 18 April 2020
0360-1323/Published by Elsevier Ltd.

to the job site until panels were unwrapped and exposed to weather [9].

Several studies have provided insight through field monitoring of CLT. McClung et al. [10] monitored the drying of various CLT wall assemblies from a wet initial condition and found that during summer and fall they dried rapidly except for cases where an impermeable membrane was placed on either side of the CLT panel. Although some monitoring studies have observed only minor variations in CLT moisture content over time [11–14], others have found that exposure to weather during construction can increase moisture levels to well above 30% MC in roof and floor panels oriented horizontally [9,15–19]. Moreover, subsequent installation of an impermeable membrane on one side of the panels resulted in slow drying [9], similar to prior findings for walls [10]. Additional studies have exposed CLT specimens outdoors to investigate differences between CLT and other wood products [20]; moisture distribution in CLT by three-dimensional imaging [21]; and effectiveness of protective coatings at reducing water uptake in CLT [22].

Laboratory characterization of CLT hygrothermal behavior is preliminary in nature [23–27]. While considerable literature exists on hygrothermal properties of various wood species [28–30], the performance of CLT panels may depend on many factors including the geometrical characteristics of the wood layers; the presence of cracks, edge gaps, and wane pockets; the type of adhesive between layers of wood; and the use of different wood species. For example, water absorption rates for full-panel specimens measured by partial immersion [24] were considerably greater than those for small specimens cut from the same panel types [25]; it is unclear whether the difference in water absorption rate was a result of the difference in scale (small clear specimens vs. panels having gaps between boards, checks, and cracks) or the difference in the method used to seal the edges of the specimens. A recent investigation of a full-scale CLT panel oriented horizontally in an environmental chamber, with exposure to wetting and drying cycles, found that water uptake from the top surface was highly variable by location, and moisture accumulated primarily at the interface between the upper two layers and near end grain, gaps, and joints [31].

Hygrothermal modeling is an important tool for building envelope analysis. CLT modeling, however, is currently limited by the preliminary nature of laboratory measurements and the lack of material properties in modeling software. WUFI software [32], for example, does not include North American CLT in its material database. Although it does include CLT from European manufacturers, the liquid transport coefficients are not specified. In addition, research is needed to validate hygrothermal models for CLT. For instance, Lepage [24] modified existing wood material properties in a hygrothermal model to achieve agreement with laboratory water uptake and drying measurements on CLT panels. Building on this work, McClung et al. [10] found that simulated CLT wall moisture contents generally agreed well with field measured data at levels below about 25% MC, but simulations tended to over-predict moisture levels in the center of the CLT panels. Additional simulations using a stochastic approach [33] further extended this work. Although these efforts achieved reasonable agreement between simulated and measured moisture contents, the coefficient for moisture redistribution was adjusted by 12 orders of magnitude. This unconventional adjustment followed the approach of Krus and Vik [34], who empirically fitted moisture transfer measurements in clear wood in the axial direction (parallel to grain), whereas the CLT studies mentioned above investigated moisture transfer perpendicular to grain (across the thickness of the panel). Moisture transfer parallel to grain can occur more than an order of magnitude faster than perpendicular to grain. In addition to these issues, it remains to be seen whether a simpler, more conventional modeling approach would provide satisfactory agreement with measurements.

Given the lack of information for hygrothermal modeling of CLT, this paper presents laboratory measurements and modeling for a type of CLT panel that was monitored in a companion study of an eight-story mass timber building in Portland, Oregon [9]. The objectives of this work are (1) to measure the hygrothermal properties needed as model inputs for simulation of CLT; (2) to conduct laboratory experiments on the wetting and drying behavior of CLT panels; (3) to implement the hygrothermal properties in a straightforward manner and validate the model using laboratory measurements; and (4) to investigate the accuracy of the model in simulating CLT moisture content in comparison to field measurements. Water uptake was measured in two configurations: one with the bottom surface immersed in water and the other using a new method with ponded water on top of the CLT panel. Drying measurements following water uptake also included two configurations: one with the wetted surface exposed to air and the other with an impermeable membrane covering the wetted surface, but with the opposite surface exposed to air. The specific contributions of this study include a new complete set of hygrothermal properties for CLT, laboratory wetting and drying measurements on CLT panels with a new procedure, implementation of the CLT properties in WUFI software using a simplified approach, a method to calibrate the liquid transport coefficient for CLT, and validation of the model with laboratory and field measurements. The modeling approach can be extended to other wood species with known properties and other CLT layups.

2. Material hygrothermal characterization

2.1. CLT material

CLT samples were off-cuts from panels produced for the construction of a mass timber building that was monitored in a companion study [9]. Six different CLT samples were obtained from the factory. Two samples (914 mm × 914 mm as received) were trimmed for large-scale tests; the other four samples (305 mm × 305 mm) were machined to produce specimens for small-scale tests as described in the next section. CLT panels were 139 mm thick and consisted of five layers (Fig. 1): four layers of wood from the spruce-pine-fir (SPF) group and one layer of Douglas-fir (DF). The layers were laminated using a polyurethane adhesive without edge gluing. Lumber used in production of the CLT panels was sourced from mills across the central interior region of British Columbia, Canada. Douglas-fir (*Pseudotsuga menziesii*) was confirmed using microscopic wood identification on several samples selected from different panels. Douglas-fir in the CLT samples was primarily heartwood. SPF lumber in the panels was primarily sapwood. Microscopic wood identification was conducted on 14 samples randomly selected

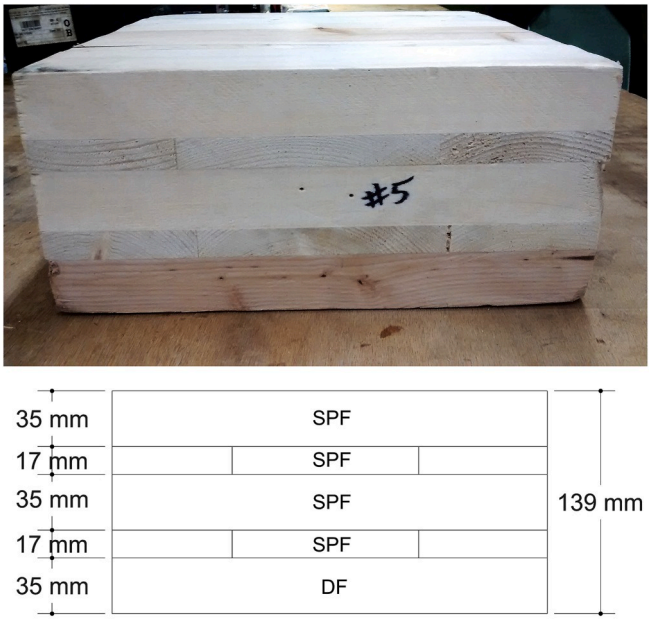

Fig. 1. One of the CLT samples used for making small-scale specimens (top); schematic cross-section (bottom).

from the top four layers of different panels. The majority were spruce (genus *Picea*) and the rest were from the yellow pine group (within the genus *Pinus*).

2.2. Measurement overview

Hygrothermal characterization of the material involved several types of laboratory measurements conducted on two different size scales. "Large-scale" specimens measured 610 mm × 610 mm × 139 mm (full panel thickness). "Small-scale" specimens were machined from four original panels to varying sizes depending on the experiment. These specimens were further divided into SPF material from a single layer, SPF material from two wood layers with the adhesive layer included, and DF material. The small-scale specimens included wood from one board in a given layer; edge gaps between boards were not included at this scale. Small specimens did, in some cases, include features such as knots and checks. The different experiments, size scales, and specimen parameters are summarized in Table 1. Details of the experimental procedures and respective results are given in the following sections.

2.3. Small-scale characterization

2.3.1. Bulk density

Dry bulk density was determined using Method A of ASTM D2395 [35] for small SPF and DF specimens cut to a variety of sizes, with length varying between 56 and 143 mm, width between 25 and 102 mm, and thickness between 13 and 33 mm. Mass was measured with an electronic balance (±0.001 g) after drying in a convection oven at 105 ± 1 °C for a minimum of 24 h (subsequent measurements at 48 h changed by no more than 0.1%). Dimensions were measured with a digital caliper (±0.01 mm). The dry bulk density of SPF was 426 ± 62 kg m^{-3} (standard deviation), close to the design value of 420 kg m^{-3} [36]. The measured value for DF was 477 ± 52 kg m^{-3}, slightly lower than the Douglas Fir-Larch group design value of 500 kg m^{-3} [36].

2.3.2. Moisture storage

The moisture storage function in the hygroscopic region (sorption isotherm) was characterized using ASTM C1498 [37], with departures noted below. Specimens were divided into two groups: one starting dry (absorption) and the other starting wet (desorption). Each group was then divided into five subgroups for placement in mechanically conditioned chambers at relative humidity (RH) conditions of 30%, 50%, 65%, 80%, and 90%, all at 23.0 ± 0.5 °C. Groups of specimens were conditioned concurrently rather than running all specimens through absorption and desorption cycles sequentially. Absorption specimens were dried at 65 °C and <1% RH prior to conditioning at the various RH levels. Desorption specimens were submerged in water for 7 days; the 76 mm × 70 mm × 12 mm blocks absorbed an appreciable amount of water, and wood cell walls were likely saturated prior to humidity conditioning. Specimens were allowed to reach constant mass at each condition, defined as three successive values at 24 h intervals differing by no more than 0.2% (which is equivalent to a rate of change in moisture content dM/dt of less than 0.6 μg of moisture per gram of dry wood per minute, for comparison with other criteria [38]). Specimens were then oven dried at 105 ± 1 °C for a minimum of 24 h. Equilibrium moisture content (EMC) was calculated as

$$\mathrm{EMC} = \frac{m_{tot} - m_{dry}}{m_{dry}} \quad (1)$$

where m_{tot} is total mass of the specimen at moisture equilibrium and m_{dry} is mass of the oven-dry specimen. EMC values are expressed in percentage dry basis (equivalent to g water per 100 g dry material). A small amount of mold growth was observed on some of the specimens at the 90% RH condition, but this had a negligible effect on the EMC.

The capillary region was characterized using the pressure plate technique following ASTM C1699 [39]. Samples were initially vacuum saturated under deionized water (3.7 kPa, 30 min). The 6 mm thickness in the longitudinal direction allowed for rapid saturation. Specimens were divided into two groups, each having 12 SPF specimens and 12 DF specimens, such that two conditions could be run simultaneously. The following applied pressures were used, listed with corresponding RH values at 22 °C: 0.14 bar (99.99% RH), 0.50 bar (99.96% RH), 1.4 bar (99.90% RH), 5.0 bar (99.63% RH), and 13.8 bar (98.99% RH). Equilibrium was attained when the total water flow from the pressure plate extractor was less than 0.05 mL over 48 h. In addition, saturation moisture content was measured (12 specimens of each wood type) by allowing specimens to absorb water while freely immersed until reaching constant mass (three successive values at 24 h intervals differing by no more than 0.05%).

EMC data are plotted in Fig. 2 as a function of relative humidity (expressed as a decimal). In the hygroscopic region the absorption EMC values are fairly close to the generic sorption isotherm from the *Wood Handbook* [29]. Desorption values are greater than absorption values as expected.

2.3.3. Water vapor diffusion

Moisture transfer in the hygroscopic region was characterized using ASTM E96 [40], with modifications noted below. Wood specimens were sealed with butyl tape to the face of a Pyrex dish containing either A3 molecular sieve desiccant (0% RH) or deionized water (100% RH). Specimens were oriented such that vapor transmission occurred perpendicular to the wood grain, primarily in the radial direction. Specimens included SPF from one layer, SPF from two layers with adhesive included, and DF. The dish assemblies were placed in an environmental chamber at 23.0 ± 0.1 °C and constant RH, either 50% or 70%, controlled to within ±2% RH (sensor calibration accuracy). Relative humidity conditions across the specimens (dish/chamber) included 0%/50%, 100%/50%, and 100%/70%. The dish assembly was removed briefly from the chamber for mass measurements (±0.01 g) at 24 h intervals until steady state was reached. The vapor permeability δ_p of the specimen was calculated as

Table 1
Summary of characterization experiments and sampling.

Measurement	Scale	Material	Specimen Dimensions (mm)	Number of Replicates	Number of Source Panels
Bulk density	Small	SPF	Various	33	4
		DF	Various	13	4
	Large	Full panel	140 × 140 × 139	7	2
Thermal conductivity	Large	Full panel	610 × 610 × 139	2	2
Moisture storage, hygroscopic	Small	SPF	76 × 70 × 12	64	4
		DF	76 × 70 × 12	52	4
Moisture storage, capillary	Small	SPF	25 × 25 × 6	24	4
		DF	25 × 25 × 6	24	4
Water vapor diffusion	Small	SPF	165 × 114 × 19	4	4
		SPF, adhesive	133 × 114 × 19	4	4
		DF	165 × 114 × 19	4	4
Liquid water absorption, partial immersion	Small	SPF	51 × 51 × 25	4	4
		SPF, adhesive	51 × 51 × 35	4	4
		DF	51 × 51 × 25	4	4
	Large	Full panel	610 × 610 × 139	2	2
Liquid water absorption, inundation	Large	Full panel	610 × 610 × 139	2	2

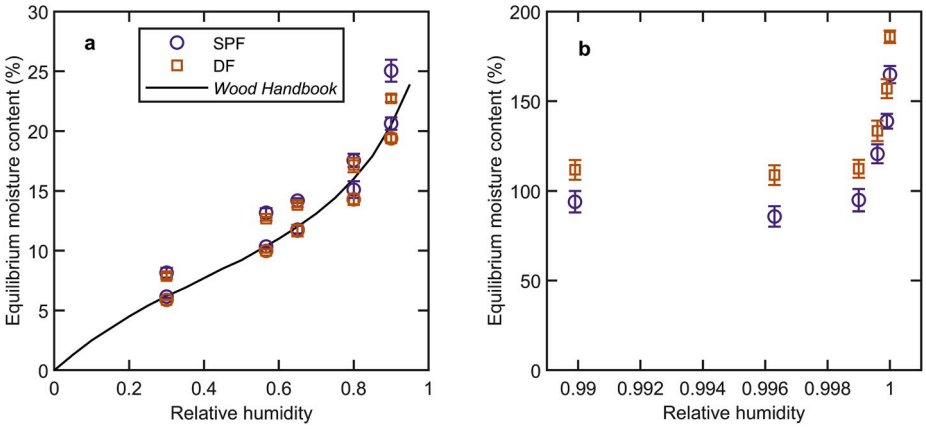

Fig. 2. Measured EMC in the hygroscopic region (a) and capillary region (b). Error bars represent one standard deviation. Note the different axis scales in each figure.

$$\delta_p = \frac{\dot{m} \cdot d}{A \cdot \Delta p_v} \tag{2}$$

where $\dot{m}$ is the steady-state mass transfer rate (kg s^{-1}), d is the specimen thickness (m), A is the exposed surface area of the specimen (m^2), and Δp_v is the difference in vapor pressure across the specimen (Pa). The vapor diffusion resistance factor μ was calculated as

$$\mu = \frac{\delta_a}{\delta_p} \tag{3}$$

where δ_a is the vapor permeability of still air (2.01×10^{-10} kg m^{-1} s^{-1} Pa^{-1} calculated for the site conditions of 23 °C and barometric pressure of 98.6 kPa). Measurements were corrected to account for still air diffusion resistance (inside the dish), surface resistances on both sides of the specimen, and edge masking of the specimen by the sealant, as recommended in the standard [40].

Results are summarized in Table 2. Specimens from the SPF group were more vapor permeable than DF, and the presence of an adhesive layer between SPF layers had a significant influence. An unpaired *t*-test was performed at each RH level to compare the vapor diffusion resistance factors of SPF specimens with and without an adhesive layer. The difference was significant at mean RH levels of 75% RH and 85% RH ($p = 0.024$ and $p = 0.001$, respectively). For a mean level of 25% RH, the difference was not significant ($p = 0.43$). The difference at higher relative humidity levels is likely a result of the relative influence of the adhesive layer because the vapor resistance of wood decreases with increasing RH conditions.

For comparison, the vapor permeability results of Alsayegh et al. [25] for CLT specimens made from western Canadian SPF are listed in Table 2. These values are lower than those found in this study for specimens of the same wood type with adhesive included. This may be a result of different species within the SPF group, different adhesives, differences in wood density, or differences in the extent of checks and cracks within the specimens.

Table 2
Measured water vapor diffusion properties.[a]

Study	Material	Mean RH (%)	Vapor Permeability (ng Pa^{-1} s^{-1} m^{-1})	Vapor Diffusion Resistance Factor
This work	DF	25	1.32 ± 0.46	171 ± 77
		75	9.3 ± 3.0	23.0 ± 5.7
		85	11.2 ± 1.0	18.1 ± 1.5
	SPF	25	1.46 ± 0.35	146 ± 41
		75	12.4 ± 5.1	17.9 ± 5.8
		85	18.7 ± 4.4	11.3 ± 2.9
	SPF (with adhesive)	25	1.21 ± 0.15	168 ± 20
		75	8.2 ± 1.2	25.0 ± 3.8
		85		
Alsayegh et al. [25]	SPF (with adhesive)	25	0.4	
		75	3.9	
		85	5.7	

[a] Error bars represent one standard deviation.

2.3.4. Liquid water absorption

Liquid water absorption was characterized using a capillary uptake test under partial immersion based on ASTM C1794 [41]. One departure from this method was the specimen size (Table 1), which gave a smaller surface area than the minimum in the standard. Specimens were oriented such that water absorption was perpendicular to the wood grain. Specimen edges were sealed using neoprene paint, which had been found in prior work to be sufficiently impermeable to water and suitable for wood specimens that expand upon moisture uptake [42]. Specimens were pre-conditioned at 50 ± 5% RH. The specimens were placed with the exposed surface immersed 3–5 mm in a tray of water maintained at a constant level. Specimens were removed periodically, blotted with a moist sponge to remove free water droplets, and weighed (±0.001 g). The water uptake through the exposed surface (kg m^{-2}) was plotted against the square root of time and was found to be approximately linear over a period up to 24 days (Fig. 3). The water absorption coefficient A_w (kg m^{-2} $s^{-1/2}$) was determined from the slope of the linear regression.

As shown in Fig. 3, SPF absorbed water faster than DF. SPF specimens with an adhesive layer showed an apparent reduction in water absorption relative to SPF specimens without adhesive, but an unpaired *t*-test indicated that the difference was not significant ($p = 0.076$). The A_w value for SPF with adhesive (2.3 g m^{-2} $s^{-1/2}$) was similar to the value measured by Alsayegh et al. [25] for the same material type (1.9 g m^{-2} $s^{-1/2}$). The plots in Fig. 3 also indicate a slight change in slope near the end of the experiment; the cause of this is not known.

2.4. Large-scale characterization

2.4.1. Bulk density

Bulk density was determined for large-scale specimens using a similar procedure to small specimens. Mass was measured (±0.01 g) after drying in an oven at 105 ± 1 °C for a minimum of 24 h, until subsequent measurements at 4 h intervals changed by no more than 0.02%. The dry bulk density of full-thickness specimens was 423 ± 28 kg m^{-3}. This value is within 1% of the density of the small-scale SPF specimens but about 13% less than DF. The measured value is about 4% less than the value calculated from SPF and DF mean densities and volume fractions within the panel, likely a result of additional void space created by gaps between boards in the panels.

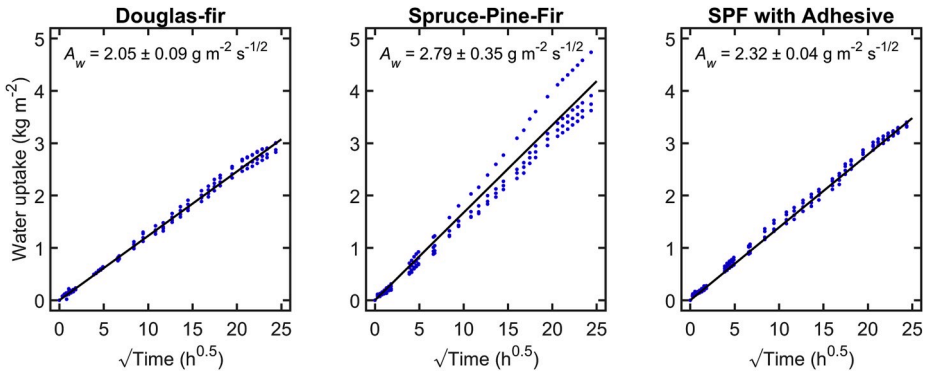

Fig. 3. Measured liquid water uptake in small-scale specimens, with mean A_w value and standard deviation for four replicates of each material type.

2.4.2. Thermal conductivity

Thermal conductivity was characterized following ASTM C518 [43] at a mean temperature of 24 °C. The top and bottom sides of the CLT panel specimen were maintained at 14 °C and 34 °C, respectively, and heat flux was measured on each side until the values converged at steady-state. Prior to thermal conductivity measurements, specimens were weighed and probed with a moisture meter to estimate moisture content, which was 10–12%. Measured values were 0.112 ± 0.003 and 0.110 ± 0.003 W m^{-1} K^{-1}. Thermal conductivity was calculated based on estimated moisture content and density using the relationship in the *Wood Handbook* [29]; values were 0.115–0.119 W m^{-1} K^{-1}. Measured and calculated values differ by 8% or less, which is within the range expected from variability in specimen density.

2.4.3. Water absorption by partial immersion

Water absorption in full CLT panels was characterized with a partial immersion experiment similar to the small-scale measurements, using a procedure adapted from Lepage [24]. The four sides of each panel specimen were coated with an impermeable liquid-applied membrane (Bituthene Liquid Membrane), which was allowed to fully cure prior to partial immersion in water (Fig. 4). An impermeable liquid-applied membrane was the most reliable of different membrane types in prior work by Lepage [24]. Specimens were pre-conditioned at 50 ± 5% RH and oriented such that water was absorbed perpendicular to the wood grain through the exposed SPF surface of the panels. Specimens were removed from water periodically for weighing (±1 g). After 30 days, the panel specimens were allowed to air dry for 24 days at laboratory conditions of 23–25 °C and 45 ± 5% RH with periodic weighing. Temperature and RH were monitored hourly (HOBO UX100-011, Onset Computer Corp., Bourne, MA, USA).

In addition to total water uptake, wood moisture content was measured at specific locations using electrical-conductance-type sensors (Model S-2, OmniSense LLC, Ladys Island, SC, USA). A prior laboratory calibration yielded measurement uncertainty of ±2% MC for the same CLT panels [9]. The sensor electrodes (stainless steel screws) were installed in the specimens from the non-wetted DF surface to varying depths (Fig. 5). Screw threads were removed except at the tip, and shafts were electrically insulated so that measurements indicated moisture conditions near the tips. After the specimens were removed from water, sensor electrodes were installed to monitor the wetted layer during the drying process (Fig. 5).

The measured water uptake was approximately linear versus the square root of time, and the A_w values for the two CLT panel specimens were 2.5 and 2.8 g m^{-2} s$^{-1/2}$, consistent with the range for small-scale SPF specimens of 2.79 ± 0.35 g m^{-2} s$^{-1/2}$ (Fig. 3). MC sensors embedded in the CLT panel specimens indicated that liquid water did not reach the electrodes 38 mm from the wetted surface during the 30-day duration of the partial immersion test.

Fig. 4. Apparatus for measurement of water absorption by partial immersion.

2.4.4. Water absorption by inundation

After partial immersion, the same CLT panel specimens were flipped so that the SPF surface faced upward. Water was absorbed from the top surface in the inundation experiment (Fig. 6). This configuration was chosen to represent exposure of a horizontal CLT floor or roof panel to rain during construction. The reservoir was constructed using an acrylic plastic dam sealed to the top surface of the panel with neoprene caulking

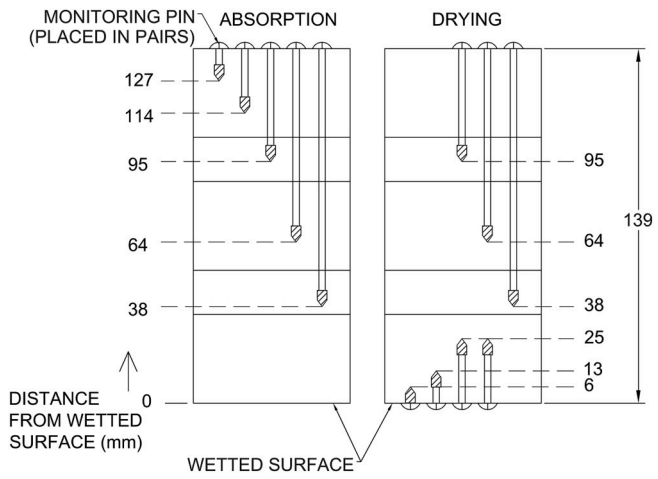

Fig. 5. Placement of electrodes for measurement of wood moisture content.

Fig. 6. Apparatus for measurement of water absorption by inundation.

and multiple layers of neoprene paint. Electronic moisture sensors were removed from the top surface during the inundation experiment, and screw holes were filled with wax.

Water was introduced to the reservoir (approximately 1.7 kg) such that the entire surface of the panel was covered to a depth of at least 3 mm. The panel assembly was leveled using lag screws. The assembly was weighed periodically; prior to each weighing, all excess water was removed with a shop vacuum; after each weighing, fresh deionized water was added to the reservoir. After 10 days of water inundation, excess water was removed, the panel assembly was weighed, and electronic moisture sensors were reinstalled on the top surface (same as Fig. 5, flipped). This surface was then covered with 0.15 mm polyethylene film to investigate drying and moisture redistribution in the panel, mimicking the effect of installing an impermeable layer after wetting during construction. The drying results are discussed below in Section 4.

Water absorption was approximately linear with the square root of time for the inundation experiment, and the A_w values for the two CLT panel specimens are listed in Table 3. Absorption coefficients determined for the inundation experiment were greater than partial immersion for the same panel specimens (Table 3). Water was observed infiltrating cracks and gaps in the CLT, resulting in a larger surface area for absorption. Moreover, some of the additional surface was likely end-grain, which is known to have a higher rate of water absorption [29].

3. Hygrothermal model description

3.1. Model overview

Software used in this study was WUFI® Pro v6.2 [32], a tool for simulation of one-dimensional transient heat and moisture transfer in multi-layer building assemblies. The model was developed by Künzel [44,45] and has been validated for many types of building assemblies. Although WUFI has been used in previous studies of CLT [10,22,24], this study takes a different approach to implementing some of the material properties. The following sections describe the material properties used as model inputs and their relationship to laboratory measurements. Properties of DF and SPF layers differed, so each material type was separately defined in the software. The materials were then combined in layers using the proper thickness to represent a CLT panel. Adhesive layers were not included in the model. The properties of SPF and DF for use in simulation software are included with this article as XML files (see *Supplementary Data*).

3.2. Density, specific heat capacity, and thermal conductivity

Dry bulk density of DF and SPF were based on laboratory measurements. Specific heat capacity and thermal conductivity of the materials in the dry state were taken from the literature [29]. These parameters are summarized in Table 4. Specific heat capacity was based on a temperature of 20 °C. The model includes the effect of moisture on heat capacity but neglects the effect of temperature. Measured thermal conductivity values under laboratory conditions were reasonably consistent with literature values (Section 2.4.2). The dry thermal conductivity values were calculated based on bulk density [29] for a mean temperature of 10 °C. The effect of temperature on thermal conductivity was included with a coefficient of 2×10^{-4} W m^{-1} K^{-2}. The effect of moisture on thermal conductivity was handled using a 1.7% increase per 1% increase in moisture content, based on the literature [29].

3.3. Moisture storage function

The moisture storage function relates water content (kg m^{-3}) and relative humidity (0–1). Water content was calculated from EMC (dry mass basis) and dry bulk density. Model values for DF and SPF were based on the measured EMC data in the hygroscopic and capillary regions. The model does not account for hysteresis; in the hygroscopic region the mean measured values for absorption and desorption were fitted using a parabolic equation [46,47]:

Table 3
Liquid water absorption coefficients for partial immersion and inundation experiments.

Panel	A_w (g m^{-2} s$^{-1/2}$)			
	Inundation Trial 1	Inundation Trial 2	Inundation Mean	Partial Immersion
1	3.6	3.1	3.4	2.5
2	3.7	3.4	3.6	2.8

Table 4
Model inputs: bulk density (measured), specific heat capacity (literature), and thermal conductivity (dry material, literature).

Wood Type	Dry Bulk Density (kg m^{-3})	Specific Heat Capacity (J kg^{-1} K^{-1})	Thermal Conductivity (W m^{-1} K^{-1})
DF	477	1237	0.111
SPF	426	1237	0.101

$$\frac{h}{m} = Ah^2 + Bh + C \tag{4}$$

where h is relative humidity (0–1), m is EMC (kg kg^{-1}), and A, B, and C are fitting parameters. The design curves and the average measured EMC values for DF and SPF are plotted in Fig. 7a and b. The design curves in the capillary region (Fig. 7c and d) were based on pressure plate measurements and free water saturation tests. Values are compared with literature pressure plate data for North American spruce and pine [48–51].

3.4. Vapor diffusion resistance factor

The model nominally partitions moisture transfer between vapor diffusion (this section) and capillary water transport (next section). Measurements for many hygroscopic materials show an increasing vapor permeability with RH. For wood this is attributed to combined vapor diffusion through the cellular structure and bound water diffusion through the cell wall; the point at which capillary condensed water begins to contribute is disputed. The vapor diffusion resistance factors of DF and SPF were assigned constant values between 0% and 25% RH, corresponding to the measured dry cup value (Table 2). Between 25% RH and 80% RH, the values were based on a curve fit to the measurements using an exponential decay function:

$$\mu = ae^{-bh} \tag{5}$$

where μ is the vapor diffusion resistance factor, h is relative humidity, and a and b are fitting parameters. The design curves for DF and SPF are shown in Fig. 8 along with the measured values. Between 80% RH and 100% RH, the vapor diffusion resistance factor was held constant; 80% RH is the default point in the model at which liquid transport begins, as described in the next section.

3.5. Liquid transport coefficients

The model includes a coefficient for suction, when the material is absorbing water, and a coefficient for redistribution, when an exterior liquid water source is absent. A simplified approach incorporated in the software was used to approximate the liquid transport coefficient for suction D_w (m^2 s^{-1}) as a function of water content w (kg m^{-3}), based on the experimental liquid water absorption coefficient A_w (kg m^{-2} s$^{-1/2}$):

$$D_w = k \cdot \left(\frac{A_w}{wf}\right)^2 \cdot 1000^{\left(\frac{w}{wf}\right)-1} \tag{6}$$

where k is a factor with an initial value of 3.8 and w_f is the water content at free saturation (kg m^{-3}). Liquid transport was included in the model when the water content was greater than or equal to the equilibrium water content at 80% RH.

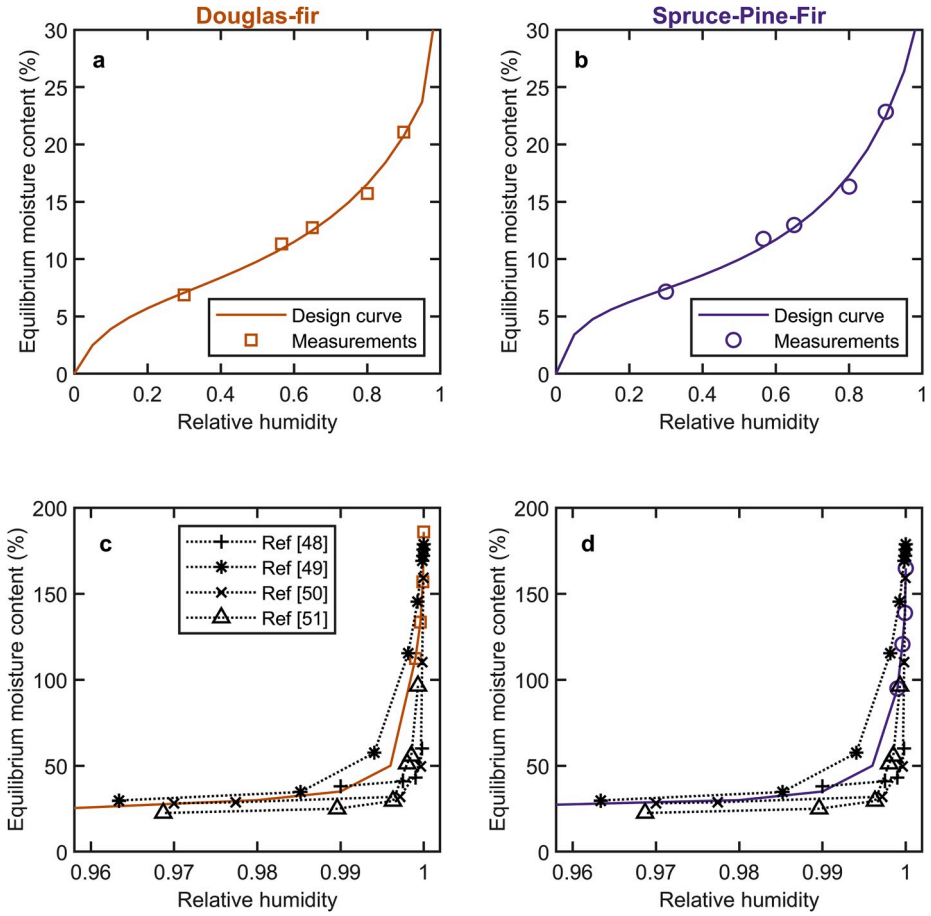

Fig. 7. Moisture storage function in the hygroscopic region for DF (a) and SPF (b); data points represent mean of absorption and desorption measurements at each RH. Moisture storage function in the capillary region for DF (c) and SPF (d) together with literature data.

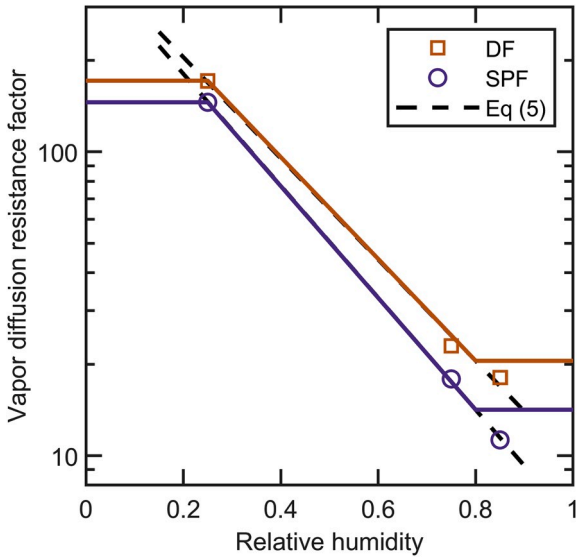

Fig. 8. Vapor diffusion resistance factors for DF and SPF as a function of relative humidity.

The adequacy of this approach was tested by comparing simulations with the small-scale water absorption measurements (Section 2.3.4), similar to the approach of Scheffler et al. [52]. The measured and simulated water uptake values are plotted in Fig. 9. The initial simulation over-predicted the rate of water absorption. A simulation with capillary water transport disabled ($D_w = 0$) suggested that vapor diffusion made a significant contribution (dashed line in Fig. 9). This was confirmed by an additional simulation (not shown) in which vapor diffusion was effectively disabled by setting the vapor diffusion resistance factor arbitrarily large. This behavior is not found in other building materials. In masonry materials, for example, capillary water absorption is dominant; it is generally much faster than water absorption in wood, and its contribution to water uptake is such that vapor diffusion is negligible in comparison. The original research that developed WUFI primarily focused on masonry materials [44]. Given the vapor diffusion contribution identified here, the factor k in Eq (6) was then modified so that the simulated water uptake matched the data; a value of $k = 2.2$ gave the best fit to measured data (dashed-dotted line in Fig. 9).

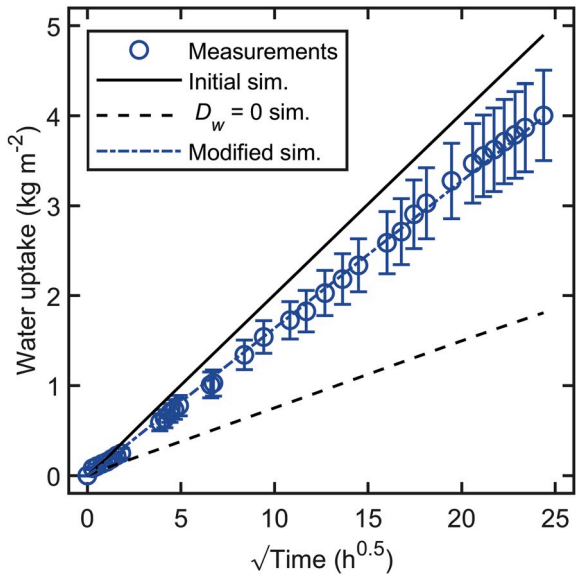

Fig. 9. Measured and simulated water uptake in small-scale SPF specimens. Error bars represent one standard deviation (four replicates).

4. Model validation

4.1. Water absorption and subsequent drying

The measured water absorption by partial immersion of the large-scale specimens (Section 2.4.3) was simulated using the approach detailed above. The mean measured A_w value for the two panel specimens was used, with $k = 2.2$ in Eq (6) based on the findings above. The boundary conditions for the surface immersed in water during the wetting period were set in the modeling software as continuous rainfall (1000 kg m^{-2} h^{-1}) to provide no limit on the water available for absorption (note that effects of gravity and hydrostatic pressure are not included). Additionally, relative humidity at the wetted surface was set to 100% and temperatures were set to hourly measured values in the laboratory. The boundary conditions at the non-wetted surface were set to hourly measured temperature and RH values. Radiation exchange and wind were neglected. During the drying period, boundary conditions at both surfaces corresponded with hourly measured temperature and RH, and surface resistances were set to zero. The liquid transport coefficient for redistribution was identical to the value for suction (Eq (6)) for simplicity.

Measured and simulated water uptake values are plotted in Fig. 10a. The simulation captures the shape of the measurements, with the largest discrepancy being an underestimation of the absorption rate near the beginning of the experiment. The simulated peak water uptake and the shape of the drying curve depended on the initial moisture content of the CLT; better agreement was reached using measured initial MC instead of estimated values. The root-mean-square deviation (RMSD) between simulated and mean measured uptake over the wetting and drying periods was 0.16 kg m^{-2}. This value is similar to the scatter in the measurements: the RMSD between measured values for the two panels was 0.24 kg m^{-2}.

The water inundation experiment (Section 2.4.4) was simulated using the same approach as above (Fig. 10b), but with the inundation A_w value rather than the partial immersion A_w value. After the ponded water was removed and the wetted surface was covered with polyethylene film, the measurements and simulations both indicated a greatly reduced drying rate (Fig. 10b) in comparison to unimpeded air drying (Fig. 10a). After seven months of air drying in the laboratory following inundation, only 36%–40% of the total water absorbed had dried from the panels. Over the simulated wetting and drying period, the RMSD between simulated and mean measured uptake for the two panels was 0.24 kg m^{-2}, which again is similar to the RMSD of 0.28 kg m^{-2} between measured values for the two panels.

4.2. Moisture profiles

In addition to accurately simulating water uptake and drying, a model should correctly predict the moisture profile through the thickness of the panel over time. Moisture contents measured with electrodes installed at various distances from the wetted surface are compared to simulated values in Fig. 11. The left column of Fig. 11 plots values for the partial immersion experiment at three points in time (refer to Fig. 10a): 31 days (just after wetting was finished and sensors were installed); 35 days (after 4 days of drying); and 54 days (after 23 days of drying). Similarly, the right column of Fig. 11 plots values for the inundation experiment. To complement the profiles in Fig. 11, moisture contents at three specific depths are plotted as a function of time in Fig. 12. As mentioned previously (Section 2.4.3, Fig. 5), the sensors measuring at depths of 25 mm or less from the wetted surface were installed after wetting was completed. The simulations capture the general shape of the measured values, the drop in moisture content as a result of air drying after partial immersion, and the slow redistribution of moisture

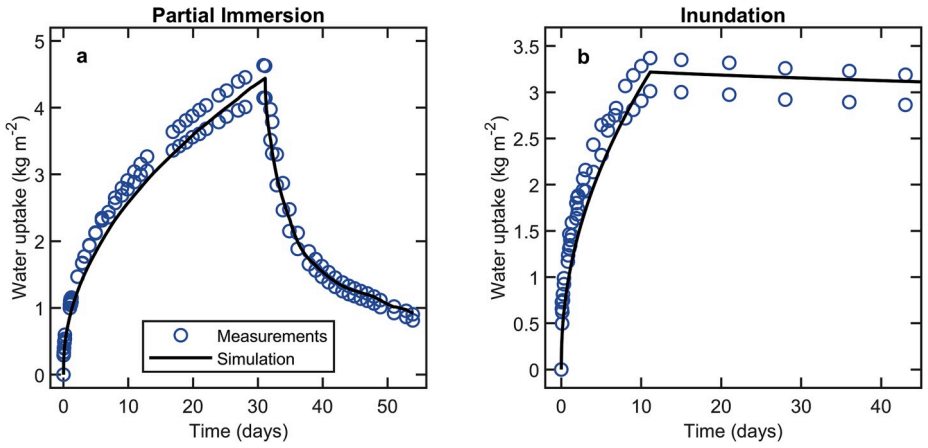

Fig. 10. Measured and simulated water uptake for partial immersion followed by air drying (a) and inundation followed by covering wetted surface with polyethylene film (b).

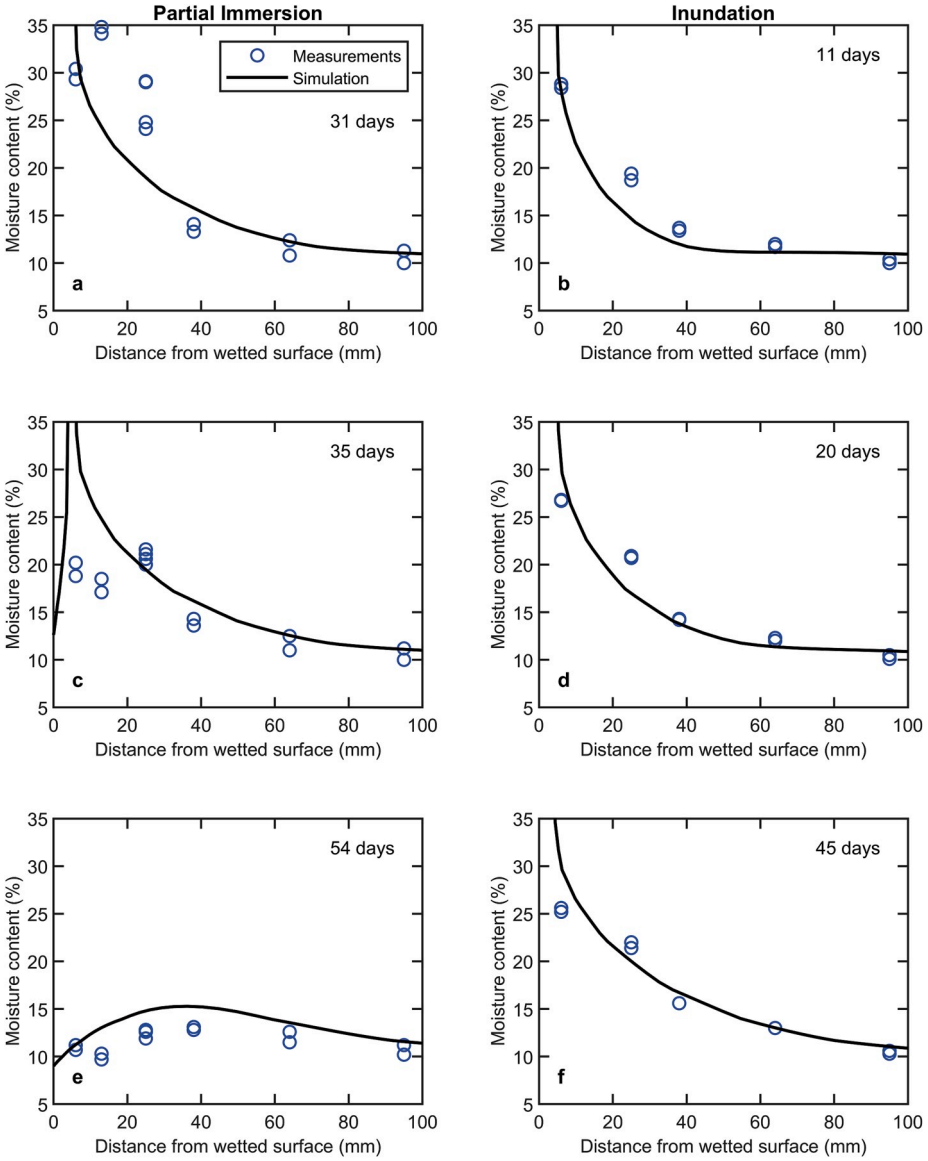

Fig. 11. Measured and simulated moisture content profiles at various points in time during the partial immersion experiment (a, c, e) and the inundation experiment (b, d, f).

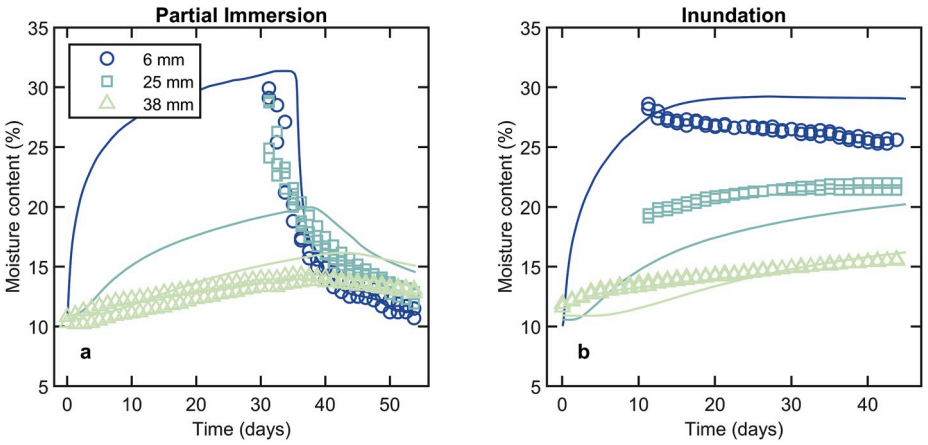

Fig. 12. Measured (markers) and simulated (lines) moisture content at specific depths versus time during the partial immersion experiment (a) and the inundation experiment (b). For clarity every 30th measured value is plotted.

following inundation and covering of the wetted surface with polyethylene film. However, there are sizeable differences between measured and simulated values for pins with high readings between 6 mm and 25 mm from the wetted surface. The limitations and uncertainties in the moisture pin readings need to be considered. Calibration of the sensors was done in a range below 26% MC; readings above this level are extrapolated and therefore approximate. Additionally the actual depth of the sensor readings has an inherent uncertainty. The screw electrodes were insulated except for a few millimeters at the tip in the attempt to measure MC at a specific depth. However, the insulation material might not have been completely robust to screw installation, removal, and reinstallation. Sensors might have had electrical contact with a larger wood volume than intended; if so they would have registered the lowest resistance (highest MC) in contact with both screws. These limitations are important to consider with the steep moisture gradient near the wetted surface.

5. Model application to building envelope assembly

5.1. Roof assembly description

The low-slope compact roof assembly of an eight story mass timber building in Portland, Oregon, was monitored in a companion study [9]. The building, instrumentation, and measurements are described in detail in that study [9]. CLT roof panels were overlaid with a vapor barrier/air barrier membrane, rigid insulation, cover board, and roof membrane (Fig. 13). An array of wireless moisture sensors (identical to those detailed in Section 2.4.3) were installed in various locations to monitor moisture content in CLT panels over time, starting from the installation of the panels. The building owner wanted sensors to be hidden from view, and because the bottom side of the CLT served as the exposed ceiling of the interior space below, it was not possible to install sensors from the underside. Instead, sensors were installed from the top side within a small notched pocket that was subsequently covered with waterproofing. Completion of the roof assembly was delayed for two months after sensor installation, and CLT roof panels were exposed to high levels of precipitation prior to application of the roof membrane. A temporary protective enclosure was built above the CLT roof, and fans were operated to dry the roof panels for one week before completion of the roof enclosure in April 2017. Despite efforts at waterproofing the sensor pockets, many of the sensors suffered water damage and data loss. For the purpose of comparison with hygrothermal simulation, measurements are presented here for a group of five sensors that recorded data continuously. These sensors were installed with insulated electrodes located in each of the five layers of the CLT roof panel.

5.2. Modeling approach

The roof assembly was simulated in the modeling software using the CLT properties described previously, together with properties of other materials taken either from manufacturer specifications or generic materials in the WUFI material database. Relevant material properties are summarized in Table 5. The exterior boundary conditions in the simulation used hourly weather data averaged from several Portland weather stations near the project site and hourly interior temperature and RH measured in the building [9]. The initial MC of each CLT layer in the model was set to be identical to the measured value at the time the assembly was completed (April 10, 2017); values from top to bottom were

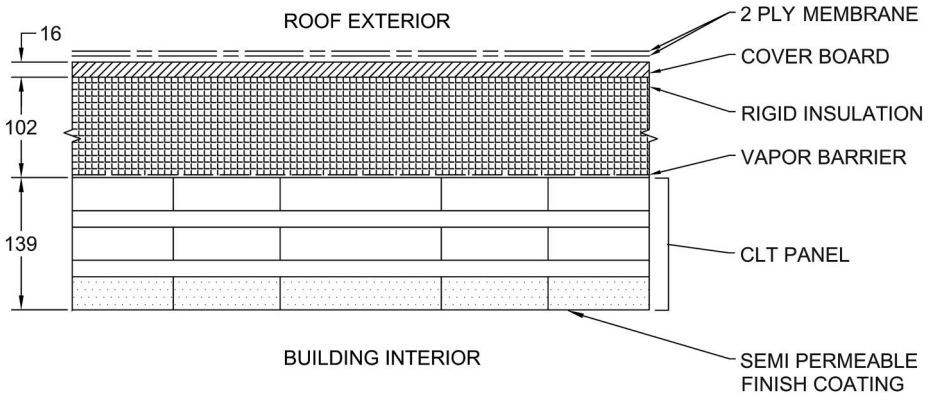

Fig. 13. Cross-section of roof assembly (dimensions in mm).

Table 5
Material properties used in simulation of roof assembly.

Material	Description	Density (kg m^{-3})	Specific heat capacity (J kg^{-1} K^{-1})	Thermal Conductivity (W m^{-1} K^{-1})	Vapor diffusion resistance factor
Roof membrane	1.5 mm	1500	[a]	[a]	30,000
Cover board	Glass fiber-faced gypsum	770	870	0.13	6.7
Rigid insulation	Polyisocyanurate foam	32	1470	0.024	69
Vapor barrier	0.76 mm	730	[a]	[a]	280,000

[a] Thermal properties of thin layers do not affect simulation outcome.

32% MC (Layer 1), 19% MC (Layer 2), 20% MC (Layer 3), 18% MC (Layer 4), and 16% MC (Layer 5). The semi-permeable finish on the interior DF surface was modeled using an interior surface mass transfer resistance corresponding to an equivalent still air thickness (*sd* - value) of 1.4 m (identical to a vapor permeance of 140 ng Pa^{-1} s^{-1} m^{-2}). The roof membrane was white and had a solar absorptivity of 0.2.

5.3. Measurements and simulation results

The measured and simulated moisture content in each layer of the CLT roof panel are compared in Fig. 14. Measurements and simulations for Layers 1, 3, 4, and 5 are mostly within the ±2% MC sensor uncertainty, although the drying rate of Layer 1 is under-predicted by the model (RMSD of 1.4% MC and maximum difference of 2.6% MC). This under-prediction of drying rate was observed in WUFI modeling of a western Canadian SPF CLT wall assembly in comparison to field measurements [10]. The largest discrepancy in Fig. 14 is Layer 2, which reaches a considerably higher moisture content in the simulation than in the measured data (maximum difference of 4.7% MC). The rise in simulated MC of Layer 2 comes from redistribution of moisture from Layer 1. The actual sensor installation, however, had a small pocket notched in the top CLT layer for sensor placement. This air pocket above Layer 2 was not included in the model.

6. Discussion

The results of this study indicate that CLT wetting and drying can be approximately described using a simplified implementation of moisture transfer properties in a one-dimensional hygrothermal model. This modeling approach could be extended to different CLT configurations, such as layups with different layer thicknesses. The approach could also be extended to CLT panels made from different wood species with known hygrothermal properties.

A significant finding of this study was that modeling liquid water absorption in wood required an adjustment of the equation used to calculate the liquid transport coefficient (Section 3.5). The default simulation over-predicted the rate of moisture uptake because vapor diffusion was found to have a significant contribution in parallel with liquid transport, which is not usually seen in other building materials. The liquid transport coefficient was tuned so that the simulated water uptake matched the data. We recommend that future modeling work include this check and that further work be done to characterize both vapor diffusion and liquid water transport for additional wood species. In addition to steady-state vapor transmission measurements, time-dependent vapor sorption measurements on specimens of different size scales would provide data for testing the modeling approach presented here.

Specimen size scale did not significantly affect liquid water absorption rates under partial immersion in this study. Individual A_w values for small SPF specimens were between 2.3 and 3.3 g m^{-2} s$^{-1/2}$, and values for CLT panels (with absorption into SPF) were 2.5–2.8 g m^{-2} s$^{-1/2}$. The additional surface area created by gaps between boards in CLT panels apparently did not significantly increase the rate of water absorption under partial immersion, compared with small specimens that lacked such features. This result is consistent with tests conducted by Lepage [24] on water absorption in clear SPF lumber specimens; 1.6 mm and

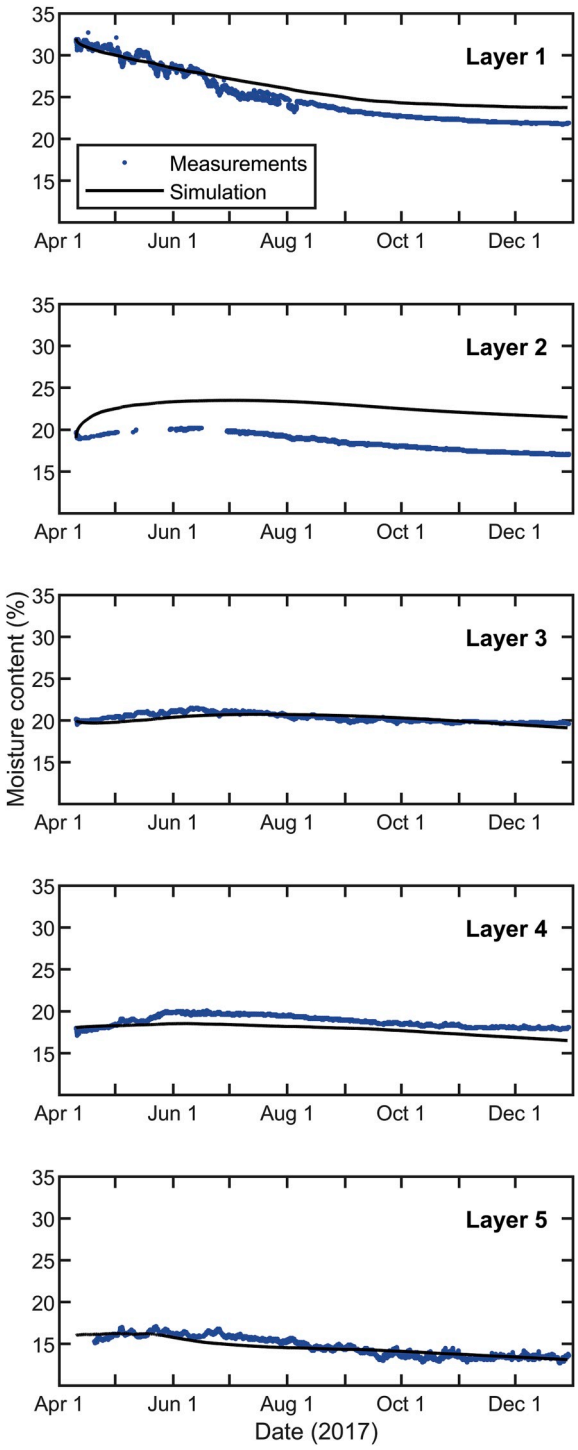

Fig. 14. Measured and simulated moisture content in each layer of CLT in the roof assembly (Layer 1: top SPF layer; Layer 5: bottom DF layer).

3.2 mm wide saw cuts across the face of the specimens did not significantly change the A_w value.

Contrary to these results, other prior studies have observed differences in A_w values between small specimens and large CLT panels. Alsayegh et al. [25] reported an A_w value of 1.99 g m^{-2} s$^{-1/2}$ for small specimens cut from CLT panels made from eastern Canadian SPF. In contrast, Lepage [24] reported a value of 5.3 g m^{-2} s$^{-1/2}$ for large CLT panels of the same type. The reason for this difference is unclear. It is unlikely that the discrepancy was caused by the edge-sealant for the CLT panels because a liquid-applied membrane was used in the case of eastern SPF [24], similar to the sealant used in this study. In other cases, CLT panels were edge-sealed with a self-adhering membrane that was reportedly not fully effective at preventing water absorption at panel edges; absorption at end-grain may have significantly increased the total water uptake. For example, the A_w value of 12 g m^{-2} s$^{-1/2}$ for western SPF CLT (self-adhering membrane) was more than twice the value of 5.3 g m^{-2} s$^{-1/2}$ for eastern SPF CLT (liquid-applied membrane) [24].

The rate of water absorption with ponded water on the top side of the CLT panel ("inundation") was significantly higher than the rate under partial immersion in this study. Water quickly infiltrated cracks and gaps in the CLT, resulting in a larger surface area, and some of the additional surface was likely end-grain, which is known to have a higher rate of water absorption. This finding is consistent with observations of Schmidt et al. [31], who noted that gaps between boards in the first layer in certain locations interfaced with gaps between boards in the second layer as well as wane. They found that water sprayed on the top side of a CLT panel led to moisture penetrating and accumulating in these locations.

Modeling CLT panels in one-dimension will not account for three-dimensional effects such as those mentioned above. Additional three-dimensional effects include swelling and shrinkage of wood as its moisture content changes. This attribute of wood could potentially alter the moisture transfer in CLT panels; for example, as the surface dries out, gaps may open up between boards and checks and cracks may develop, all resulting in greater surface area. These phenomena may explain why the model under-predicts drying rates, as mentioned in Section 5.3.

Another limitation of this work is neglecting the effect of the adhesive layer on moisture transfer. This was done for simplicity and because the measurements were not conclusive regarding the effect of the adhesive, given the limited number of replicates. The adhesive layer provided a significant resistance to vapor diffusion under high RH conditions but not under low RH conditions. The effect of the adhesive layer on water absorption was not significant. We recommend that more extensive work be done in future research to characterize the effects of different adhesive types on moisture transfer in CLT.

7. Conclusions

This study characterized the hygrothermal behavior of CLT panels consisting of four layers of spruce-pine-fir lumber and one layer of Douglas-fir lumber, all sourced from western Canada, using small-scale and large-scale laboratory measurements, field measurements, and modeling. Measured properties were implemented in one-dimensional transient hygrothermal simulation software (WUFI). The following conclusions can be drawn from this work.

1. Simulation of water absorption in CLT showed that vapor diffusion had a significant role in parallel with liquid transport.
2. Water absorption measured using a new method, in which the top of the CLT panel was exposed to ponded water, gave a higher rate of water uptake than the partial immersion test.
3. The rate of drying of CLT panels was much slower when the wetted surface was covered with an impermeable membrane versus exposed to air.
4. A simple approximation for liquid transport coefficients, calibrated based on measurements, with identical coefficients for suction and redistribution, was adequate for simulating panel-scale wetting and drying. Differences between measurements and simulations were on the order of the specimen-to-specimen variation for total water uptake. Simulated moisture profiles were mostly in agreement with electronic moisture measurements at specific depths in the panels, considering measurement uncertainties.
5. Finally, hygrothermal simulations of a CLT roof assembly were compared with measurements over a nine-month period from a companion field study of an eight-story mass timber building in Portland, Oregon. With the exception of one CLT layer, the simulations were mostly within about ±2% MC of the measurements.

Declaration of competing interest

The authors declare that they have no known competing financial interests or personal relationships that could have appeared to influence the work reported in this paper.

Acknowledgments

This work was supported by the U.S. Forest Service [Grant 16-DG-11020000-060]. The authors gratefully acknowledge the materials and assistance provided by Kris Spickler and Steve Bamford of Structurlam. The authors thank Alex Wiedenhoeft of the U.S. Forest Products Laboratory (FPL) for wood identifications. This article was improved by helpful comments from Robert Lepage of RDH Building Science, Marco Lo Ricco of FPL, and anonymous reviewers.

Appendix A. Supplementary data

Supplementary data to this article can be found online at https://doi.org/10.1016/j.buildenv.2020.106866.

References

[1] M. Mohammad, S. Gagnon, B.K. Douglas, L. Podesto, Introduction to cross-laminated timber, Wood Des. Focus 22 (2) (2012) 3–12.
[2] E. Karacabeyli, B. Douglas, CLT Handbook: Cross-Laminated Timber, U.S. Edition, FPInnovations and Binational Softwood Lumber Council, Pointe Claire, QC, Canada, 2013.
[3] A. Iqbal, Recent developments in tall wood buildings, in: P. Mukhopadhyaya (Ed.), 1st International Conference on New Horizons in Green Civil Engineering, University of Victoria, Victoria, BC, Canada, 2018, pp. 111–116.
[4] J.E. Jakes, X. Arzola, R. Bergman, P. Ciesielski, C.G. Hunt, N. Rahbar, M. Tshabalala, A.C. Wiedenhoeft, S.L. Zelinka, Not Just Lumber—Using Wood in the Sustainable Future of Materials, Chemicals, and Fuels, JOM 68 (9) (2016) 2395–2404, https://doi.org/10.1007/s11837-016-2026-7.
[5] S. Gagnon, C. Pirvu, CLT Handbook: Cross-Laminated Timber, FPInnovations, Québec, QC, Canada, 2011.
[6] G. Finch, J. Wang, D. Ricketts, Guide for Designing Energy-Efficient Building Enclosures for Wood-Frame Multi-Unit Residential Buildings in Marine to Cold Climate Zones in North America, FPInnovations, Vancouver, BC, Canada, 2013.
[7] E. Karacabeyli, C. Lum, Technical Guide for the Design and Construction of Tall Wood Buildings in Canada, FPInnovations, Vancouver, BC, Canada, 2014.
[8] ANSI/APA, PRG 320-2018, Standard for Performance-Rated Cross-Laminated Timber, APA–The Engineered Wood Association, Tacoma, WA, USA, 2018.
[9] S. Kordziel, S. Pei, S.V. Glass, S. Zelinka, P.C. Tabares-Velasco, Structure moisture monitoring of an 8-story mass timber building in the Pacific Northwest, J. Architect. Eng. 25 (4) (2019), 04019019, https://doi.org/10.1061/(ASCE)AE.1943-5568.0000367.
[10] R. McClung, H. Ge, J. Straube, J.Y. Wang, Hygrothermal performance of cross-laminated timber wall assemblies with built-in moisture: field measurements and simulations, Build. Environ. 71 (2014) 95–110.
[11] E. Serrano, B. Enquist, J. Vessby, Long term in-situ measurements of displacement, temperature and relative humidity in a multi-storey residential CLT building, in: World Conference on Timber Engineering, Quebec City, Canada, 2014.
[12] C. Leyder, E. Chatzi, A. Frangi, Structural health monitoring of an innovative timber building, in: Second International Conference on Performance-Based and Life-Cycle Structural Engineering (PLSE 2015), Brisbane, Australia, 2015.
[13] J. Wang, E. Karsh, G. Finch, M. Chen, Field measurement of vertical movement and roof moisture performance of the Wood Innovation and Design Centre, in: World Conference on Timber Engineering, Vienna, Austria, 2016, pp. 3120–3128.
[14] Y. Goto, K.G. Wakili, Y. Ostermeyer, A.S. Kalagasidis, H. Wallbaum, Hygrothermal performance of a vapor-open envelope for subtropical climate, field test and model validation, Build. Environ. 110 (2016) 55–64.

[15] G. Finch, High-rise wood building enclosures, in: 13th International Conference on Thermal Performance of the Exterior Envelopes of Whole Buildings, American Society of Heating, Refrigeration, and Air-Conditioning Engineers (ASHRAE), Clearwater, FL, USA, 2016, pp. 679–692.
[16] G. Mustapha, K. Khondoker, J. Higgins, Moisture performance and vertical movement monitoring of pre-fabricated cross laminate timber – featured case study: UBC Tallwood House, in: 15th Canadian Conference on Building Science and Technology, Vancouver, BC, Canada, 2017.
[17] G. Mustapha, K. Khondoker, J. Higgins, Structural performance monitoring technology and data visualization tools and techniques—featured case study: UBC Tallwood House, in: 1st International Conference on New Horizons in Green Civil Engineering (NHICE-01), Victoria, BC, Canada, 2018, pp. 335–343.
[18] E. Schmidt, M. Riggio, Monitoring moisture performance of cross-laminated timber building elements during construction, Buildings 9 (6) (2019), 144.
[19] M. Riggio, E. Schmidt, G. Mustapha, Moisture monitoring data of mass timber elements during prolonged construction exposure: the case of the forest science complex (peavy Hall) at Oregon state university, Front. Built Environ. 5 (2019), 98.
[20] J.Y. Wang, R. Stirling, P.I. Morris, A. Taylor, J. Lloyd, G. Kirker, S. Lebow, M. E. Mankowski, H.M. Barnes, J.J. Morrell, Durability of mass timber structures: a review of the biological risks, Wood Fiber Sci. 50 (2018) 110–127.
[21] J.J. Morrell, I.N. Morrell, D. Treblehorn, A. Sinha, Moisture intrusion in cross laminated timber and the potential for fungal attack, in: World Conference on Timber Engineering, Seoul, Republic of Korea, 2018.
[22] R. Lepage, J. Higgins, G. Finch, Moisture uptake testing for CLT floor panels in a tall wood building in Vancouver, in: 15th Canadian Conference on Building Science and Technology, Vancouver, BC, Canada, 2017.
[23] Y. Goto, K. Ghazi Wakili, Y. Ostermeyer, T. Frank, N. Ando, H. Wallbaum, Preliminary investigation of a vapor-open envelope tailored for subtropical climate, Build. Environ. 46 (3) (2011) 719–728.
[24] R.T.M. Lepage, Moisture Response of Wall Assemblies of Cross-Laminated Timber Construction in Cold Canadian Climates, Department of Civil Engineering, University of Waterloo, Waterloo, ON, Canada, 2012.
[25] G. Alsayegh, P. Mukhopadhyaya, J. Wang, E. Zalok, D. van Reenen, Preliminary characterization of physical properties of cross-laminated-timber (CLT) panels for hygrothermal modelling, Adv. Civ. Eng. Mater. 2 (1) (2013) 472–484.
[26] V. Kukk, R. Horta, M. Püssa, G. Luciani, H. Kallakas, T. Kalamees, J. Kers, Impact of cracks to the hygrothermal properties of CLT water vapour resistance and air permeability, Energy Procedia 132 (2017) 741–746.
[27] J. Tripathi, Hygrothermal Properties of Cross Laminated Timber Panels, School of Forest Resources, University of Maine, Orono, ME, USA, 2017.
[28] M.K. Kumaran, J.C. Lackey, N. Normandin, F. Tariku, D. van Reenen, A Thermal and Moisture Transport Property Database for Common Building and Insulating Materials: Final Report from ASHRAE Research Project 1018-RP, American Society of Heating, Refrigerating and Air-Conditioning Engineers, Inc., Atlanta, GA, 2002.
[29] S.V. Glass, S.L. Zelinka, Moisture relations and physical properties of wood, in: R. J. Ross (Ed.), Wood Handbook—Wood as an Engineering Material, General Technical Report FPL-GTR-190, U.S. Department of Agriculture, Forest Service, Forest Products Laboratory, Madison, WI, USA, 2010.
[30] 2017 ASHRAE Handbook—Fundamentals Ch. 26: Heat, Air, and Moisture Control in Building Assemblies—Material Properties, ASHRAE, Atlanta, GA, USA, 2017.
[31] E.L. Schmidt, M. Riggio, A.R. Barbosa, I. Mugabo, Environmental response of a CLT floor panel: lessons for moisture management and monitoring of mass timber buildings, Build. Environ. 148 (2019) 609–622.
[32] WUFI® Pro, Version 6.2, Fraunhofer Institute for Building Physics, Holzkirchen, Germany, 2018.
[33] L. Wang, H. Ge, Hygrothermal performance of cross-laminated timber wall assemblies: a stochastic approach, Build. Environ. 97 (2016) 11–25.
[34] M. Krus, T.A. Vik, Determination of hygric material properties and calculation of the moisture balance of wooden prisms, in: 5th Symposium on Building Physics in the Nordic Countries, Gothenburg, Sweden, 1999, pp. 313–320.
[35] ASTM D2395-17, Standard Test Methods for Density and Specific Gravity (Relative Density) of Wood and Wood-Based Materials, ASTM International, West Conshohocken, PA, USA, 2017.
[36] NDS Supplement: National Design Specification, Design Values for Wood Construction, American Wood Council, Leesburg, VA, USA, 2018.
[37] ASTM C1498-04a(2016), Standard Test Method for Hygroscopic Sorption Isotherms of Building Materials, ASTM International, West Conshohocken, PA, USA, 2016.
[38] S.V. Glass, C.R. Boardman, E.E. Thybring, S.L. Zelinka, Quantifying and reducing errors in equilibrium moisture content measurements with dynamic vapor sorption (DVS) experiments, Wood Sci. Technol. 52 (4) (2018) 909–927, https://doi.org/10.1007/s00226-018-1007-0.
[39] ASTM C1699-09(2015), Standard Test Method for Moisture Retention Curves of Porous Building Materials Using Pressure Plates, ASTM International, West Conshohocken, PA, USA, 2015.
[40] ASTM E96/E96M-16, Standard Test Methods for Water Vapor Transmission of Materials, ASTM International, West Conshohocken, PA, USA, 2016.
[41] ASTM C1794-15, Standard Test Methods for Determination of the Water Absorption Coefficient by Partial Immersion, ASTM International, West Conshohocken, PA, USA, 2015.
[42] S.L. Zelinka, S.V. Glass, C.R. Boardman, Improvements to water vapor transmission and capillary absorption measurements in porous materials, J. Test. Eval. 44 (6) (2016) 2396–2402, https://doi.org/10.1520/JTE20150209.
[43] ASTM C518, Standard Test Method for Steady-State Thermal Transmission Properties by Means of the Heat Flow Meter Apparatus, ASTM International, West Conshohocken, PA, USA, 2017.
[44] H.M. Künzel, Simultaneous Heat and Moisture Transport in Building Components: One- and Two-Dimensional Calculation Using Simple Parameters, Fraunhofer IRB Verlag, Stuttgart, Germany, 1995.
[45] H.M. Künzel, K. Kiessl, Calculation of heat and moisture transfer in exposed building components, Int. J. Heat Mass Tran. 40 (1) (1997) 159–167.
[46] S.L. Zelinka, S.V. Glass, Water vapor sorption isotherms for southern pine treated with several waterborne preservatives, J. Test. Eval. 38 (4) (2010) 521–525, https://doi.org/10.1520/JTE102696.
[47] S.L. Zelinka, S.V. Glass, E.E. Thybring, Myth versus reality: do parabolic sorption isotherm models reflect actual wood-water thermodynamics? Wood Sci. Technol. 52 (6) (2018) 1701–1706, https://doi.org/10.1007/s00226-018-1035-9.
[48] J.E. Stone, A.M. Scallan, The effect of component removal upon the porous structure of the cell wall of wood. II. Swelling in water and the fiber saturation point, TAPPI (Tech. Assoc. Pulp Pap. Ind.) 50 (10) (1967) 496–501.
[49] C. Tremblay, A. Cloutier, Y. Fortin, Moisture content–water potential relationship of red pine sapwood above the fiber saturation point and determination of the effective pore size distribution, Wood Sci. Technol. 30 (5) (1996) 361–371.
[50] J. Zhang, P.N. Peralta, Moisture content-water potential characteristic curves for red oak and loblolly pine, Wood Fiber Sci. 31 (4) (1999) 360–369.
[51] J.Y. Wang, P. Mukhopadhyaya, P.I. Morris, Sorption and capillary condensation in wood and the moisture content of red pine, J. Build. Phys. 37 (4) (2014) 327–347.
[52] G. Scheffler, J. Grunewald, R. Plagge, Evaluation of functional approaches to describe the moisture diffusivity of building materials, J. ASTM Int. (JAI) 4 (2) (2007) 1–16.